High-resolution Rydberg-state spectroscopy of stable alkaline-earth elements

R. Beigang*

Institut für Quantenoptik, Universität Hannover, Welfengarten 1, 3000 Hannover 1, Federal Republic of Germany

Received May 12, 1988; accepted July 15, 1988

High-resolution Rydberg-state spectroscopy was applied to investigate high-lying Rydberg states of the alkaline-earth elements Mg, Ca, Sr, and Ba up to principal quantum numbers $n > 200$. In this energy range interactions dominate that are negligible at low n. It is shown that the hyperfine interaction can be used as a sensitive probe for configuration interactions, singlet–triplet mixing, and hyperfine-induced n mixing.

1. INTRODUCTION

The development of new techniques to excite and detect high Rydberg states of atoms and molecules has stimulated an increasing number of new experiments. A systematic study of a whole Rydberg series allows for the determination of interactions between the series under investigation or localized perturbations caused by single levels. From these measurements a wealth of information has been obtained, leading to an increased understanding of atomic physics. The strength of interaction will vary with principal quantum numbers n, and by choosing the appropriate energy range the desired information can be extracted with minimal perturbations from other interfering effects. In addition, the investigation of Rydberg states with extremely high principal quantum numbers n offers us the unique possibility of studying interactions that are too weak and, therefore, negligible at low n. It also facilitates the measurement of effects that scale with high powers of n.

In particular, extensive investigations of high Rydberg states of alkaline-earth elements were carried out recently by using various spectroscopic methods. Rydberg states of two-electron systems exhibit three markedly different features compared with alkali systems. First, the coupling between the two valence electrons is crucial to the properties of the Rydberg states, and in general we have to distinguish between series with predominantly singlet or triplet character. Second, two-electron systems can form two types of Rydberg series. In the main series only one electron is excited, and the second electron remains in the lowest possible configuration, resulting in Rydberg series of type $msnl$ ($l = s, p, d, \ldots$), converging to the $ms\,^2S_{1/2}$ ionization limit. If both electrons are excited simultaneously, the doubly excited series $m'l'nl'$ converges with increasing principal quantum number n to the corresponding limits $m'l'^2L_J$ of the ion. A few members of this series may lie below the first ($ms\,^2S_{1/2}$) ionization limit and cause perturbations of the regular series owing to configuration mixing. This in turn can lead to singlet–triplet mixing, affecting the whole series, or can result in perturbations that are more-or-less local in energy. The third feature involves the interaction of the nonexcited ms valence electron and the nucleus. For nuclei with a nuclear spin I, the magnetic interaction causes a hyperfine splitting as well as hyperfine-induced singlet–triplet mixing and level shifts. Because only the unpaired s electron is responsible for the magnetic interaction and the contribution of the excited electron can be neglected in first order, the hyperfine structure is sensitive to the type of coupling between the two electrons and can consequently be used as a sensitive probe for configuration interaction and singlet–triplet mixing. The interaction of the nonexcited s electron with the nucleus remains constant in first order, with increasing principal quantum number n, but depends strongly on the coupling of the two electrons. However, the energy separation between states with consecutive principal quantum numbers, singlet–triplet separations, and fine-structure splittings decreases with $1/n^{*3}$ (n^* is the effective principal quantum number). Because of this particular feature of two-electron systems, the effects investigated here can be classified into three different groups. The first group deals with experiments in which the hyperfine interaction is small compared with all other interactions mentioned above. The hyperfine structure is merely used as a sensitive probe for configuration interaction and singlet–triplet mixing. These measurements provide an unambigous test for wave functions and considerably improve analyses by means of multichannel quantum-defect theory (MQDT). With increasing principal quantum number n, the singlet–triplet separation and fine-structure splittings become comparable with the hyperfine interaction. As a result, strong interactions between neighboring Rydberg states (within the same n) are observed, and only F will remain a good quantum number. For high n this will be the rule rather than the exception. Finally, in the third group of experiments the separation between consecutive Rydberg states is comparable with the Fermi-contact term of the lower s electron. This leads to interaction between hyperfine components with different n but the same F. This type of interaction was observed for the first time in high Rydberg states of Sr. Because these interactions occur at principal quantum numbers $n > 100$, a thermionic ring diode was developed for the detection of these highly excited atoms, which allows for measurements at particularly high n without the perturbing influence of electric stray fields.

This paper is organized as follows: After a brief historical survey of Doppler-limited Rydberg-state spectroscopy, ex-

0740-3224/88/122423-14$02.00

perimental considerations for Doppler-free methods are carried out, and the experimental setup used for the research reported here is described. Results of typical experiments according to the classification scheme are reported in Section 4. All experiments reported here will deal only with states below the ionization limit, and no external magnetic or electric fields will be considered.

2. DOPPLER-LIMITED EXPERIMENTS

The determination of hyperfine structures requires, of course, Doppler-free spectroscopic techniques. In earlier measurements, Doppler-limited methods were applied to gain information about state mixing without using the hyperfine structure as the probe. These experiments are briefly reviewed here. The first measurements of Rydberg states of alkaline-earth elements were carried out by means of absorption spectroscopy with incoherent light sources (see, e.g., Refs. 1–5). From the measured level energies, the quantum defect as a function of n and the ionization limits were determined by using the Rydberg–Ritz formula.[6] The advent of pulsed, tunable dye lasers greatly increased the possibilities of investigating complete Rydberg series up to high principal quantum numbers. Because of the high spectral power density and the narrow bandwidth obtainable with dye lasers, selective stepwise excitation, or direct multiphoton transitions allowed for the determination of a great number of odd- and even-parity Rydberg series in all alkaline-earth elements.[7–20] Taking advantage of thermionic detection,[21,22] we were able to detect even high Rydberg states in a cell geometry.[23] MQDT developed by Seaton[24] turned out to be an excellent tool for the analysis and interpretation of spectra of the alkaline-earth elements. A first analysis of alkaline-earth spectra with this theory was performed by Lu,[25] who used a graphic method to fit the data. He determined the influence of the mp^2 configuration on the even-parity Rydberg states of Be, Mg, Ca, Sr, and Ba. More-sophisticated MQDT analyses were later carried out for Ca,[26,27] Sr,[28] and Ba.[29–32] In a review paper by Cooke[33] the basic aspects of the analysis obtained from level energies and MQDT are summarized.

Other quantities that are sensitive to state mixing and to the type of coupling between the two electrons have also been used successfully for Rydberg-state spectroscopy. Lifetime measurements in Ba (Refs. 34–37) and Sr (Refs. 38 and 39) reveal the strong singlet–triplet mixing between the $^1D_2$ and $^3D_2$ states. The configuration interaction of the Ba $5d7d\ ^1D_2$ state was probed by using lifetime measurements in combination with radio-frequency spectroscopy.[35] The analysis of Stark-shift measurements in Ba resulted in the determination of a $5d7d\ ^1D_2$ admixture into the main $J = 2$ series.[35] Similar experiments were performed in Sr in the energy region where the $^1D_2$ and $^3D_2$ series are strongly perturbed by interaction with the $4d6s$ configuration.[40] Ca Stark-shift experiments demonstrate the localized singlet–triplet mixing around $n = 15$. In this experiment fine-structure splittings were measured with high precision by using frequency-doubled light from a cw dye laser and an atomic beam.[41] g-factor measurements reproduced exactly the avoided crossing between $5snd\ ^1D_2$ and $^3D_2$ series in Sr around $n = 16$.[42] In Ba the perturbation due to the $5d7d\ ^1D_2$ state around $n = 26$ was clearly resolved, and the amount of perturber character in the regular series was determined.[43]

All these data provide a relatively complete picture of Rydberg states of the alkaline-earth elements Sr and Ba and to some extent also of Ca. It should be pointed out, however, that none of the quantities used for the analysis is sensitive to the relative sign of admixture coefficients of mixed wave functions. Therefore wave functions cannot be determined unambiguously. The sensitivity of all methods allows for the detection of singlet–triplet admixtures down to a few percent. Therefore, in the case of light alkaline-earth elements Ca and Mg, no singlet–triplet mixing was observed, as there is almost pure LS coupling and perturbations by doubly excited states are strongly localized.

3. EXPERIMENTAL CONSIDERATIONS

The above-mentioned experiments are not suited for the determination of hyperfine-induced perturbations, and no indication of the influence of such effects was observed. For that reason, Doppler-free spectroscopic methods have to be applied. In addition, hyperfine-structure measurements allow not only for the detection of hyperfine interactions but also for the determination of configuration interactions that are not caused by the hyperfine interaction itself.

To overcome Doppler broadening and to achieve the required resolution, a Doppler-free technique was used in combination with a narrow-band cw dye laser. The high resolution is necessary, as the separation between different isotopes and hyperfine components is of the order of 10–500 MHz. Two-photon spectroscopy is particularly well suited for the investigation of high Rydberg states in Ca, Sr, and Ba because the energy difference between the ground state and the Rydberg states can be bridged by two photons of an energy that is accessible with cw dye lasers. The output power necessary for two-photon transitions is obtainable with a ring dye laser. These laser systems are ideal tools, especially for high-resolution two-photon spectroscopy, because of the high single-mode output power and narrow bandwidth.

The measurements reported here were carried out with a commercial ring dye laser in the wavelength region between 406 and 480 nm, which was covered by three different dyes. For the spectroscopy of Ca, Sr, and Ba, Stilbene 1, Stilbene 3, and Coumarin 102, respectively, were used. All these dyes were pumped with the UV lines of an Ar^+-ion laser, providing a maximum pump power of 3.6 W. The dye laser was frequency stabilized to an external Fabry–Perot reference cavity, resulting in a linewidth of approximately 1 MHz. The total continuous single-mode tuning range extended over 30 GHz, which was more than sufficient for measurement of all hyperfine components and isotopes of one Rydberg state in a single scan. The separation between different hyperfine components or isotopes was calibrated by means of a confocal Fabry–Perot interferometer with a free spectral range of 125 MHz. In case a higher precision was necessary, a frequency-offset locking technique[44] was applied, which allows for an accuracy of better than ±150 kHz for the determination of frequency separations. A wavemeter provided a wavelength scale with an absolute accuracy of ±0.01 cm^{-1}. Thus high Rydberg states were identified unambiguously. A schematic diagram of the experimental setup is shown in Fig. 1. Details of the frequency-offset locking system and of a wavemeter with higher accuracy (±5 MHz) are given in Refs. 44 and 45.

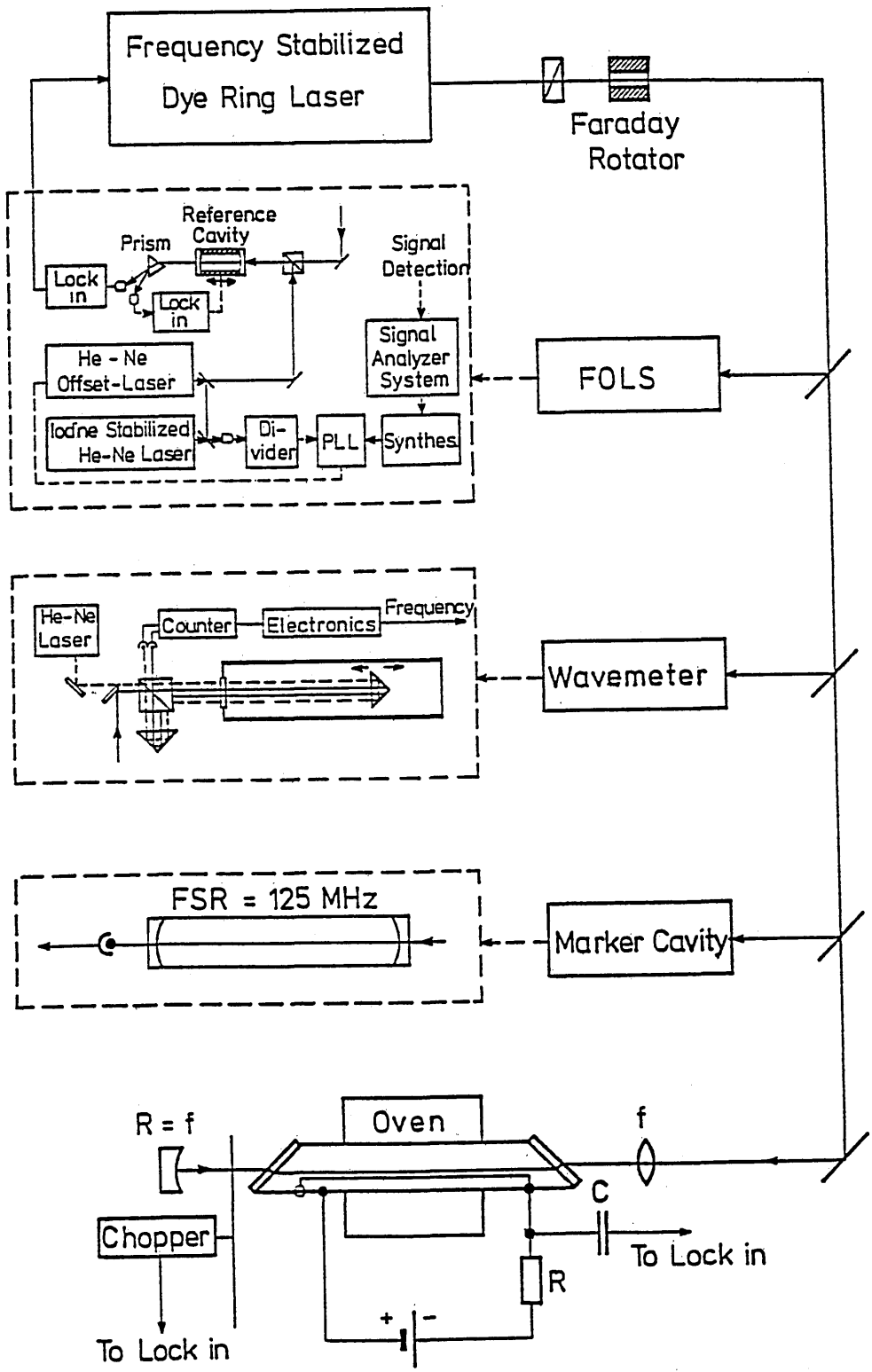

Fig. 1. Experimental setup: FOLS, frequency-offset locking system; PLL, phase-locked loop; FSR, free spectral range; f, focal length; C, capacitor; R, radius.

The metal vapor was produced in a stainless-steel heat pipe heated to a temperature that corresponds to a vapor pressure of approximately 25 mTorr. Doppler-free signals were obtained by applying the usual geometry for high-resolution two-photon spectroscopy.[46] To produce the power density necessary for the two-photon process, the beam was focused into the center of the pipe and reflected back through a spherical mirror. The excited Rydberg atoms were then detected by a space-charge-limited thermionic diode with substantial gain for detection of ionization. This detection method has proved to be particularly well suited for the spectroscopy of Rydberg states in a cell geometry.

The sensitivity increases with increasing principal quantum number and therefore partly compensates for the decreasing transition probability. The principle and the optimal operating conditions have been described in detail elsewhere.[47,48]

Typical examples of excitation spectra of $msnd\ ^1D_2$ states of Mg, Ca, Sr, and Ba obtained by Doppler-free two-photon spectroscopy and thermionic detection are shown in Fig. 2. The natural abundances of the various isotopes are also listed in the figure. For details of the spectra, see Section 4. The high detection sensitivity may be illustrated from the Ca spectrum. The intensity of the $F = 3/2$ hyperfine component of the ^{43}Ca hyperfine multiplet corresponds to an abundance of only 0.01%. From such spectra the hyperfine coupling constant can be determined easily for all alkaline-earth elements except Mg. Because of the almost pure LS coupling in Mg, a frequency-offset locking technique has to be applied to determine the small hyperfine splitting, which is caused mainly by configuration interactions, as shown in Subsection 4.B.

Other Doppler-free methods are, in principle, also suited for Rydberg-state spectroscopy. Optical–optical double-resonance techniques and stepwise excitation have been successfully applied in a cell geometry.[49] In combination with thermionic detection it is possible to excite magnetic-dipole or electric-quadrupole transitions in the first step and to reach states of different parity compared with the ground state and the second transition.[50] Both methods require two narrow-band dye lasers, and the spectra may be rather complicated owing to the intermediate level. Another widely used technique to obtain Doppler-free spectra is the application of an atomic beam. Because of the low vapor density in the beam, direct two-photon excitation is impossible, and stepwise excitation has to be employed. Thus, again, two narrow-band lasers are required. For the detection, field ionization with an electron-counting system is necessary. The electric field has to be shielded carefully from the excitation zone of the atom. With this technique, e.g., with Ba, Rydberg states were investigated up to principal quantum numbers $n = 60$.[41,51–55]

Doppler-free two-photon spectroscopy in a cell geometry with thermionic detection is considerably simpler but still more sensitive than all the methods mentioned above. It is rather straightforward to excite and detect Rydberg states with principal quantum number $n > 100$. In addition, the

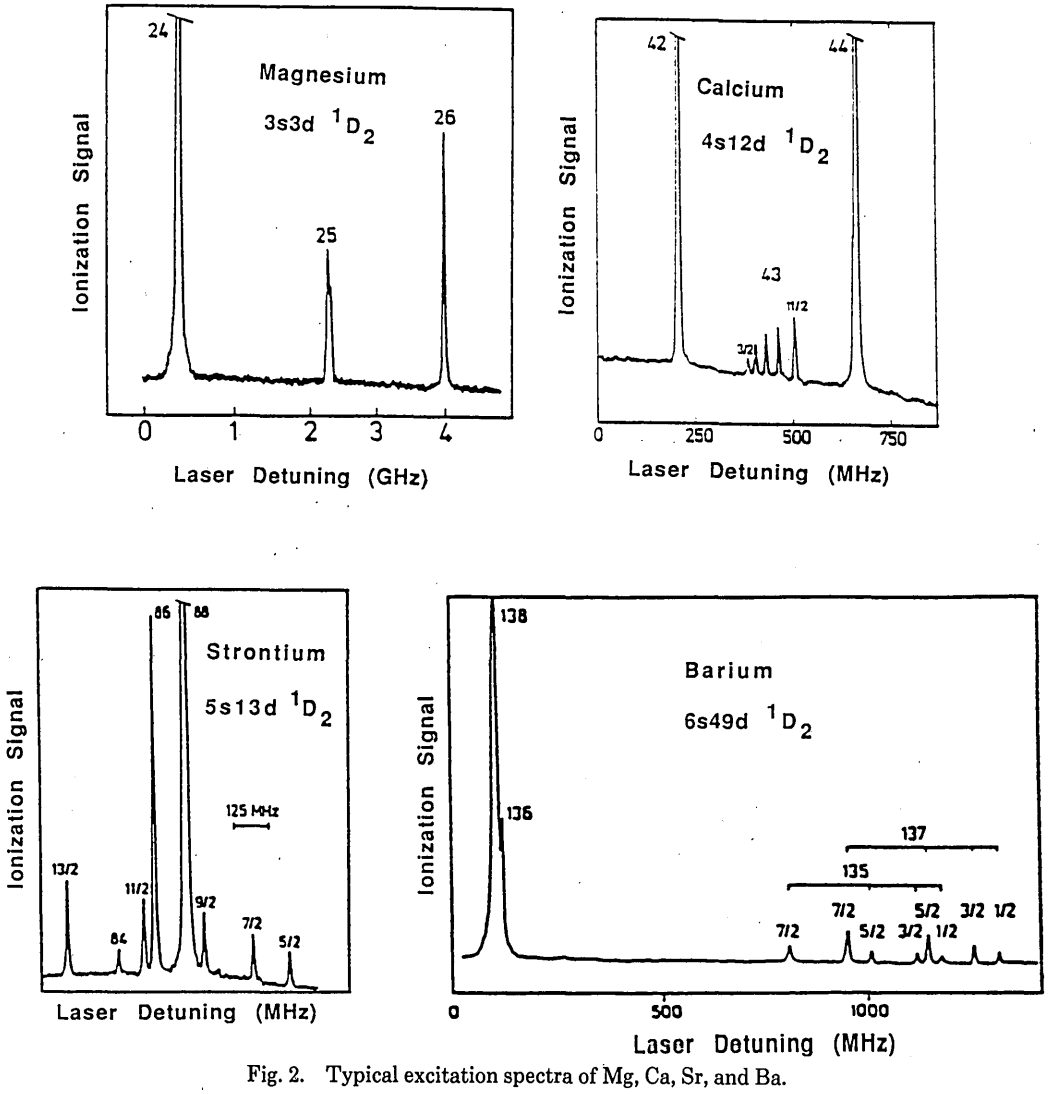

Fig. 2. Typical excitation spectra of Mg, Ca, Sr, and Ba.

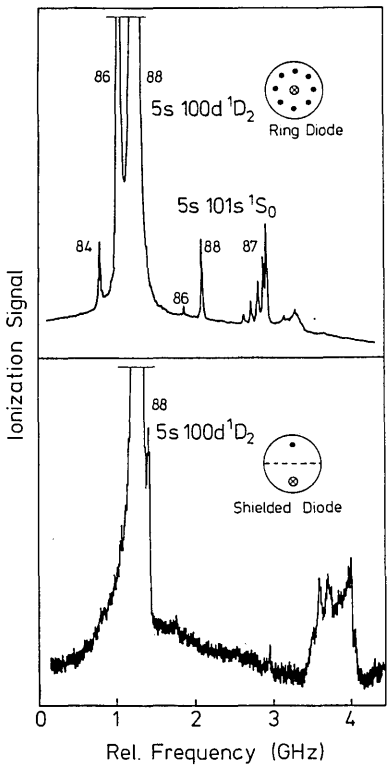

Fig. 3. Top, Two-photon excitation spectra isotopes are marked by their mass numbers. For comparison, the lower part shows the same transitions obtained with a shielded diode.

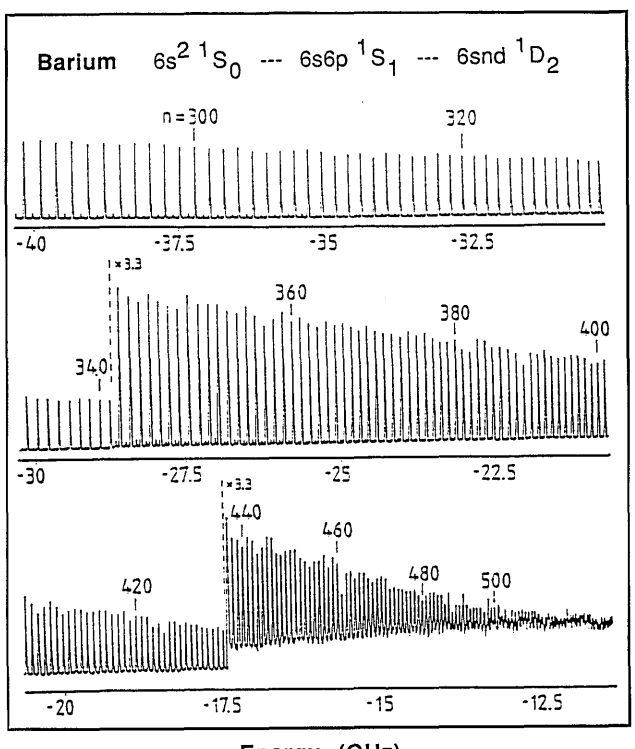

Fig. 4. Excitation spectrum of Ba Rydberg states with $n > 500$.[56]

spectra are, in most cases, not so complicated as with stepwise excitation, and only one laser is required. Note, however, that in the thermionic diode space charges produce electric fields perturbing the states under investigation. This influence becomes dominant for Rydberg states because of the high polarizability of Rydberg atoms.

For the detection of high Rydberg states, a particularly designed thermionic ring diode was applied. A thermionic ring diode considerably reduces the problems caused by electric fields and allows for high-resolution spectroscopy up to principal quantum number $n > 200$. The new device is based on an axially symmetric arrangement of the space-charge-surrounded wires with respect to the exciting laser beam and thus compensates for the influence of electric fields in first order. In addition, the detection sensitivity is also increased, owing to the geometric arrangement of the detection wires.

In practice the device consists of a number of stainless-steel wires (typically 10–12) arranged longitudinally on a radius of ~1 cm around the axis of the metal pipe, and the resulting field at the center, where the excitation takes place, is zero, owing to the radial symmetry. A typical Doppler-free two-photon excitation spectrum of the $5s\ 100d\ ^1D_2$ and $5s\ 101s\ ^1S_0$ Rydberg states of Sr is shown in the upper part of Fig. 3. All four stable Sr isotopes are clearly resolved. For comparison, the same transitions recorded with a conventional shielded diode are displayed in the lower part of the figure. The improvement when a ring diode is used is obvious. As a consequence, Rydberg states up to principal quantum numbers $n > 200$ in Sr were measured with a resolution of ~50 MHz. For such measurements close to the ionization limit the ring diode is of critical importance.

Recently the combination of atomic-beam techniques and mass-sensitive detection resulted in the excitation and observation of Rydberg states of Ba with principal quantum numbers $n > 500$. A spectrum obtained with this technique is shown in Fig. 4.[56] These extremely highly excited atoms are ideally suited for investigations of magnetic and electric field effects, and impressive effects have been shown.[56,57]

4. RESULTS AND DISCUSSION

A. General Remarks

The experiments presented here demonstrate how the hyperfine structure can be used as a sensitive probe for state mixing, hyperfine-induced singlet–triplet mixing, and interaction between states with different principal quantum numbers n at high n ($n \gg 100$). It turned out that the hyperfine structure is in particular well suited for the accurate determination of mixed wave functions, weak singlet–triplet mixing in light alkaline-earth elements (Mg and Ca), configuration interactions, and, of course, all hyperfine-induced effects. The hyperfine structure can be exploited in different ways, depending on the energy of the Rydberg states under consideration.

The total energy of an $msnl$ Rydberg state of an atom with nuclear spin I can be described by the Hamiltonian

$$H = H_{01} + H_{02} + e^2/r_{12} + \zeta_{nl}sl + a_{ms}sI, \qquad (1)$$

where H_{0i} includes the Coulomb attraction of the ith elec-

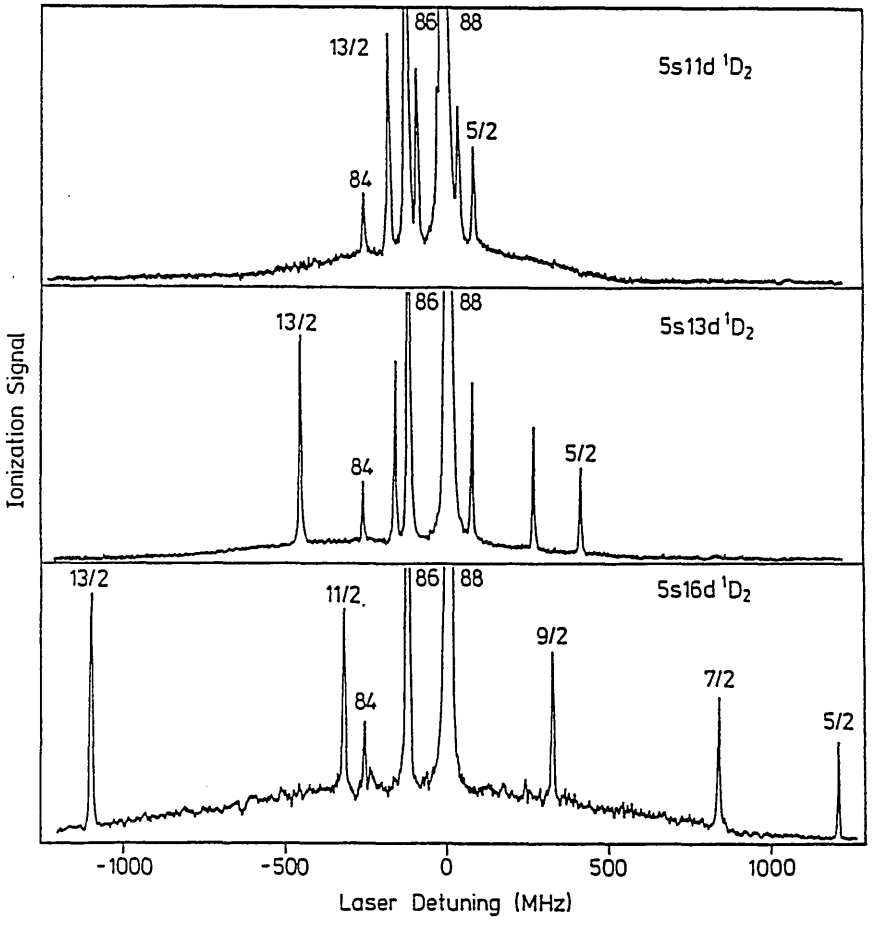

Fig. 5. Two-photon excitation spectra for $5s^2\,{}^1S_0$ and $5snd\,{}^1D_2$ transitions in natural Sr. Signals due to even isotopes are labeled by their mass numbers, whereas hyperfine components of ^{87}Sr are marked by their F values.

tron, e^2/r_{12} stands for the Coulomb repulsion between the two electrons, ζ_{nl} is the magnitude of spin–orbit interaction, a_{ms} is the magnetic interaction of the excited electron, and spin–spin and spin–other-orbit interactions are assumed to be negligible. The Fermi-contact term a_{ms} remains constant with increasing principal quantum number n of the outer electron, whereas singlet–triplet separation and fine-structure splitting decreases with $1/n^{*3}$. This characteristic feature of two-electron systems can be used to classify certain energy ranges of Rydberg series in which characteristic effects for the energy range under consideration are observed.

B. $H_{0i} \gg a_{ms}$

The magnetic hyperfine interaction is small compared with Coulomb attraction (H_{0i}), Coulomb repulsion (e^2/r_{12}), and spin–orbit interaction (ζ_{nl}). Here the hyperfine splitting serves merely as a probe for state mixing. This probe is sensitive because even high Rydberg states in the alkaline-earth elements remain predominantly LS coupled, and this coupling is crucially influenced by the admixture of other configurations.

A favorable case for an experimental test is Sr, for which Esherick[28] has shown that strong singlet–triplet mixing occurs in $5snd$ states around $n = 16$, whereas for $n \ll 10$ and $n \gg 30$ the ^1D and ^3D states can be regarded as being pure states. Wynne *et al.*[42] verified that the g factors of the $5snd$ $J = 2$ states accurately reflect the change of admixture. For

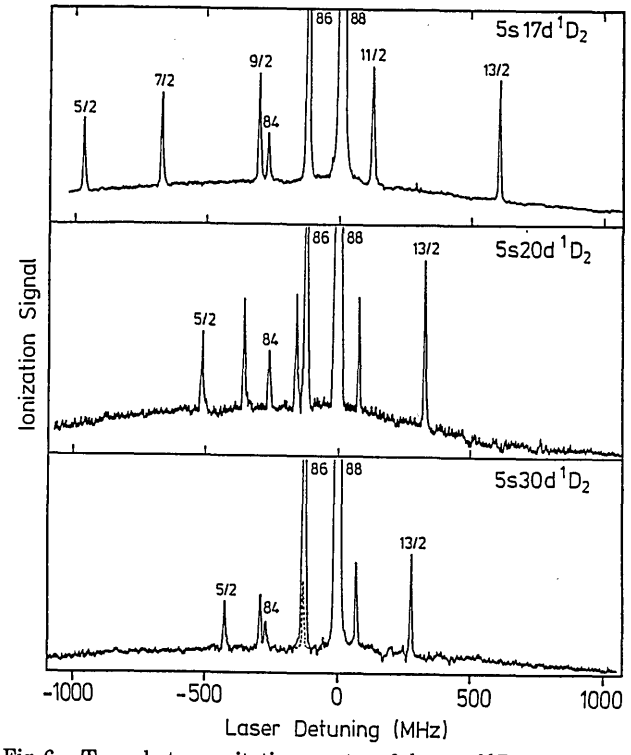

Fig. 6. Two-photon excitation spectra of the $5snd\,{}^1D_2$ series. The labeling of the lines is as in Fig. 5.

the same reason the hyperfine splitting of Sr is expected to vary with the principal quantum number between $n = 10$ and $n = 30$. A systematic study of the hyperfine splitting of the $5snd$ Rydberg states of Sr for a wide range of n demonstrates the drastic influence of singlet–triplet mixing on the hyperfine splitting. Typical excitation spectra of the $5snd$ $^1D_2$ and $^3D_2$ series are displayed in Figs. 5 and 6, respectively. The three even isotopes of Sr, with an abundance of 0.56% (^{84}Sr), 9.86% (^{86}Sr), and 77.56% (^{88}Sr), are clearly resolved, the last two ones being off scale. The interest of this investigation focuses on the five hyperfine components of ^{87}Sr ($I = 9/2$) with F values ranging from 5/2 to 13/2. The spectra in Figs. 5 and 6 were selected to demonstrate the strong dependence of the hyperfine splitting on n. In Fig. 5 the vast increase of the splitting when one is going from $n = 11$ to $n = 16$ is shown for the singlet series. The decrease of the hyperfine splitting for $n > 16$ is displayed in Fig. 6. The opposite sign of the hyperfine splitting below and above $n = 16$ is obvious from the two figures.

All hyperfine spectra obey the interval rule, and hence the quadrupole coupling constant B was assumed to be zero. Under this assumption the magnetic coupling constant A_{exp} was extracted from the spectra by applying a least-squares-fit procedure to all ten possible combinations of hyperfine intervals. The resulting data for A_{exp} are plotted as a function of n in Fig. 7b for both the triplet and singlet series. The hyperfine splitting shows a pronounced resonancelike behavior around $n = 16$, whereas it remains independent of n for $n > 30$.

For a quantitative description of the data, the intermediate-coupling scheme has to be applied for all values of n. By using the magnetic-dipole matrix elements for an sd configuration in intermediate coupling, the admixture per state can be calculated from the measured hyperfine-coupling constants. The results agree well with data obtained from MQDT analysis (Fig. 7a). For $25 < n < 40$ an admixture of approximately 2% $5snd$ $^3D_2$ into the $5snd$ $^1D_2$ states is sufficient to explain the observed hyperfine splitting.

The singlet–triplet mixing in the $5snd$ Rydberg series of Sr, as observed in these measurements, was already known from pulsed measurements and MQDT analysis,[28] whereas singlet–triplet mixing in Ca was detectable only by using the hyperfine structure as the probe.[58] Admixture coefficients smaller than 0.1% were safely detected.

In ^{25}Mg ($I = 7/2$) the influence of the $3p^2\,^1D_2$ configuration and the direct contribution of the excited d electron was determined for the $3s3d$ $^1D_2$ level.[59] Figure 8 shows the experimentally determined hyperfine splitting. The spectrum was obtained by means of the frequency-offset locking system,[21] with an accuracy of better than ±150 kHz for the determination of energy separations. A and B factors were determined to be −5.14 and 8.38 MHz, respectively. The magnetic hyperfine structure, which is zero for states with pure LS coupling, is caused partly by the admixture of approximately 20% $3p^2\,^1D_2$ character into the $3s3d$ $^1D_2$ state ($A_1 \sim -3$ MHz). The direct contribution of the excited $3d$ electron gives rise to a contribution of $A_2 \sim -0.5$ MHz, and the remaining part can be attributed to a small singlet–triplet mixing (<0.1%). For a detailed analysis of singlet–triplet mixing, higher members of the $3snd$ $^1D_2$ series and the corresponding $^3D_2$ levels have to be measured.

When mixing coefficients as determined from hyperfine-structure measurements are used, MQDT analyses can be improved considerably. This was demonstrated in the case of the Ba Rydberg series when only by using these data were we able to reproduce the singlet–triplet mixing in Ba correctly.[60,61] It should be mentioned that precise level energy measurements can also be used to evaluate even weak interactions.[45]

C. $a_{ms} \sim e^2/r_{12}$, ζ_{nl}

In the second energy range the hyperfine interaction is comparable with spin–orbit interaction ζ_{nl} and Coulomb repulsion (e^2/r_{12}) but is still small with respect to the energy separation between levels from different principal quantum numbers n. A strong mixing of neighboring Rydberg states is expected because of the hyperfine interaction, and only F

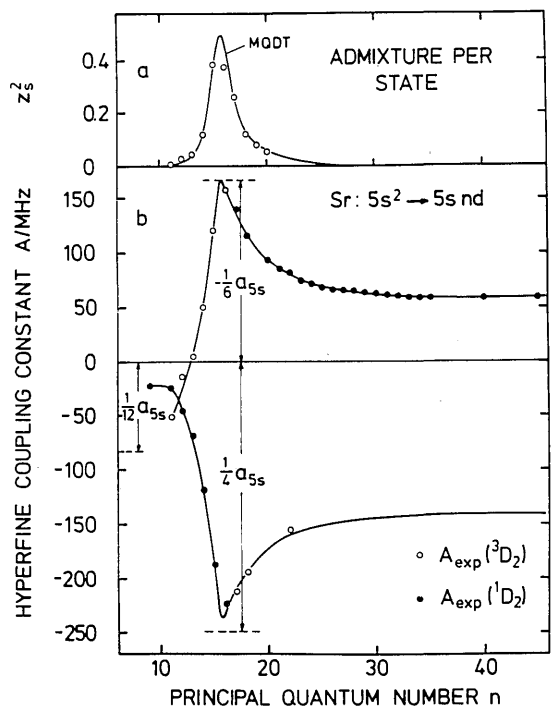

Fig. 7. a, Amount of admixture of singlet into triplet states taken from Ref. 26 (solid curve). Open circles denote the admixture per state calculated from the data shown in b. b, Observed hyperfine coupling constants for the $5snd$ $^1D_2$ (filled circles) and $^3D_2$ (open circles) states as a function of n. The solid curve represents the results of calculations using the intermediate coupling scheme. The hyperfine coupling constants for pure (jj) coupling are indicated.

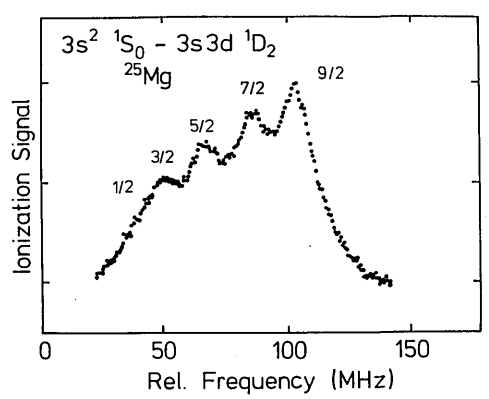

Fig. 8. Hyperfine structure of the $3s3d$ $^1D_2$ state of ^{25}Mg.

will remain a good quantum number. Such hyperfine-induced state mixing has been mentioned by Kopfermann in his book, *Nuclear Moments*.[62] When isotope shifts are neglected, hyperfine components converge to different ionization limits compared with the ones with no nuclear spin. This hyperfine-induced level shift causes singlet, as well as triplet, hyperfine components to merge into the hyperfine doublet of the $ms^2\,^2S_{1/2}$ ground state of the ion. This hyperfine-induced singlet–triplet mixing is of critical importance in particular for the character of high Rydberg states in two-electron systems, as was pointed out by Liao *et al.*[63] and independently by Barbier and Champeau.[64] Instructive examples for these effects are the *msns* Rydberg series of Ca, Sr, and Ba, and typical results will be shown below.

A quantitative calculation of the singlet–triplet shift is based on the solution of the eigenvalue problem of the perturbed Hamiltonian by using mixed wave functions. The Hamiltonian H_0 of the unperturbed system has to be extended by the Fermi-contact term $W = a_{ms}sI$.

The wave function is taken as a linear combination of the singlet and triplet wave functions, with the total angular momentum $F = I$:

$$|\psi\rangle = a_1|\psi_1(F = I)\rangle + a_3|\psi_3(F = I)\rangle. \tag{2}$$

If we diagonalize H and consider that

$$H_0|\psi_1\rangle = E_1|\psi_1\rangle \tag{3}$$

and

$$H_0|\psi_3\rangle = E_3|\psi_3\rangle, \tag{4}$$

the following secular equation for the perturbed eigenvalues E^* of H is obtained:

$$\det \begin{vmatrix} E_1 + \langle\psi_1|W|\psi_1\rangle - E^* & \langle\psi_1|W|\psi_3\rangle \\ \langle\psi_3|W|\psi_1\rangle & E_3 + \langle\psi_3|W|\psi_3\rangle - E^* \end{vmatrix} = 0. \tag{5}$$

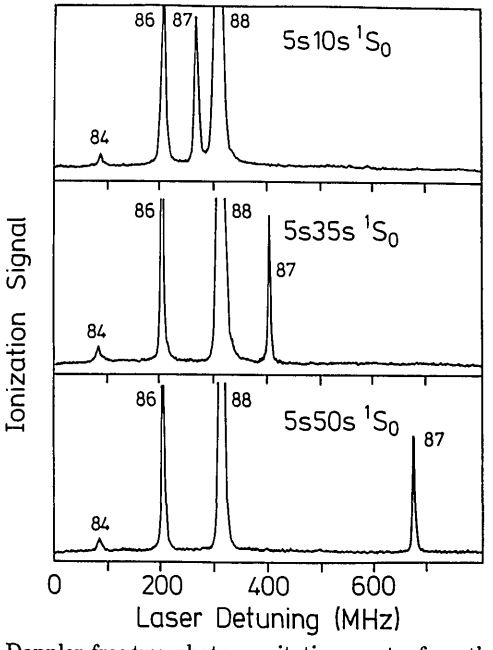

Fig. 9. Doppler-free two-photon excitation spectra from the $5s^2\,^1S_0$ Rydberg states. The isotopes are labeled by their mass numbers.

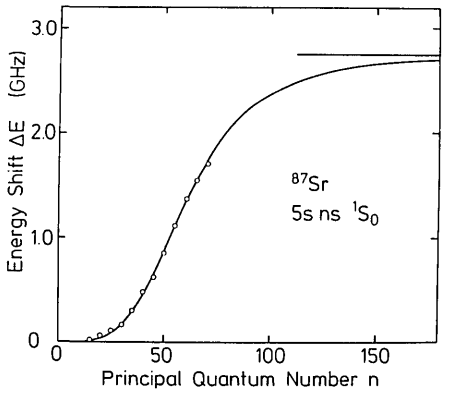

Fig. 10. Calculated energy shift for ^{87}Sr as a function of the principal quantum number n. Circles represent the experimental data.

The energy differences $\Delta E_{1/3}$ from the unperturbed term values E_1 and E_3 due to the hyperfine interaction are then given by

$$\Delta E_{1,3} = \mp(E_1 - E_3) - a_{ms}/4 \pm 1/2[(E_1 - E_3)^2 + a_{ms}(E_1 - E_3) + a_{ms}{}^2(l + 1/2)^2]^{1/2}. \tag{6}$$

Typical results for Sr, Ca, and Ba will now be discussed.

1. *Strontium*

Sr is a favorable case for the observation of the hyperfine-induced level shift. The maximum shift is rather large (2.75 GHz) so that even at low principal quantum numbers a pronounced energy shift can be observed.

Typical spectra of different *msns* $^1S_0$ Rydberg states of Sr as obtained with two-photon excitation are shown in Fig. 9. All stable Sr isotopes are resolved. The isotope shifts between even isotopes are dominated by the normal mass shift. Because they all have nuclear spin $I = 0$, there is no additional energy shift that is due to hyperfine interactions. However, the energy shift of the odd ^{87}Sr isotope, depending on the principal quantum number (as discussed above), can be observed clearly.

A comparison between experimentally obtained level shifts of the odd isotope and values calculated by using Eq. (6) is shown in Fig. 10. The experimental data were determined by measuring the isotope shift between ^{86}Sr and ^{87}Sr and by subtracting the normal mass shift. The remaining shift represents a combination of the hyperfine-induced level shift, the specific mass shift, and the field shift. The specific mass shift and field shift should show no n dependence and are neglected for Sr.[6] The theoretical curve was calculated by taking the Fermi-contact term $a_{5s} = -0.99$ GHz. The singlet–triplet energy differences as a function of n were derived by using the Rydberg formula $E_i = I_{\text{ion}} - R/(n - \delta_i)^2$ and the following parameters: $I = 45\,932.19\ \text{cm}^{-1}$, $\delta_1 = 3.269$, $\delta_3 = 3.37$. At low principal quantum numbers ($n < 30$) there is only a small increase of the energy shift, above $n \sim 30$ it increases drastically, and it finally starts to saturate at $n \sim 80$, converging to the $F = I - 1/2$ hyperfine component of the Sr II $^2S_{1/2}$ ground state, with a maximum shift of 2.75 GHz. There is excellent agreement between theory and experiment.

2. Calcium

The natural mixture of Ca contains one stable odd isotope, ^{43}Ca ($I = 7/2$), with an abundance of only 0.135 at. %. Figure 11 shows a laser scan over the $4s10s\ ^1S_0$ Rydberg state, with the well-resolved ^{43}Ca and the even isotopes ^{40}Ca, ^{42}Ca, ^{44}Ca, and ^{48}Ca again demonstrating the high detection sensitivity of the space-charge-limited thermionic diode. However, the two-photon transition probabilities for the $4sns\ ^1S_0$ series decrease drastically above $n \sim 15$ with increasing quantum number, as already observed by Wynne *et al.*[42] Thus, in the case of Ca, the isotope ^{43}Ca could only be detected up to $n = 21$ at a corresponding laser wavelength of 408.2 nm. Here the single-mode output power of the ring laser working with Stilbene 1 was limited to approximately 30 mW only. In comparison, the hyperfine components of the $4snd\ ^1D_2$ levels have been resolved up to $n = 50$ (laser wavelength $\sim$ 406 nm) with the same experimental setup.

The Fermi-contact term a_{4s} was calculated with the Fermi–Segrè–Goudsmit formula[22] to be $a_{4s} = -0.827$ GHz. In the insert of Fig. 12 the experimental data are compared with theory, showing reasonable agreement. The experimental values were obtained by applying the same procedure as for Sr. Although we did not measure high-n values, the trend for the odd–even energy shift is obvious.

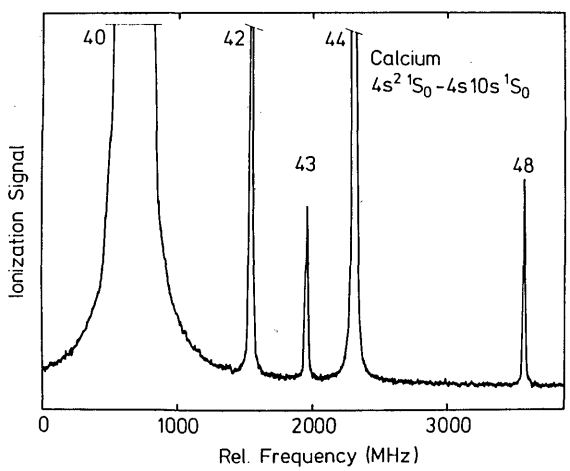

Fig. 11. Two-photon excitation spectrum for the $4s^2\ ^1S_0\ 10s\ ^1S_0$ transition in natural Ca.

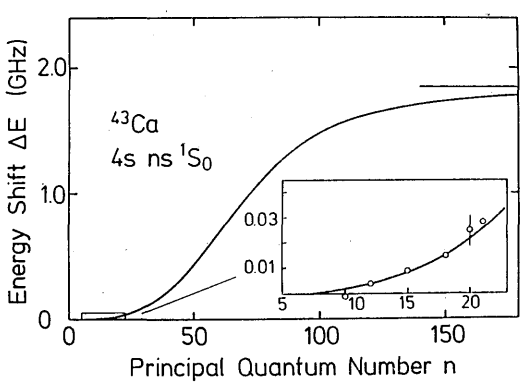

Fig. 12. Calculated energy shift for ^{43}Ca as a function of the principal quantum number n. In the inset, experimental data are compared with the prediction. The error bar represents the error intervals for all determined data.

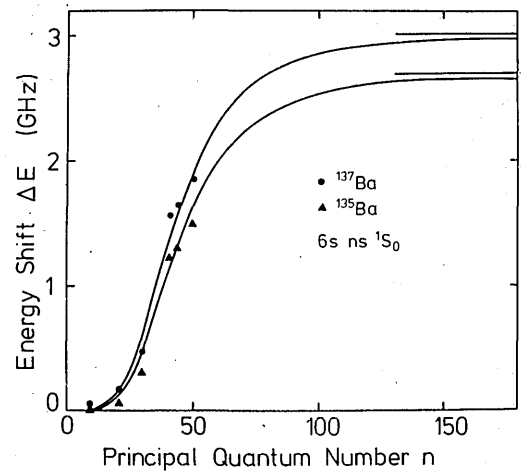

Fig. 13. Calculated energy shifts for ^{135}Ba and ^{137}Ba as a function of the principal quantum number n. Experimental data for ^{135}Ba and ^{137}Ba are added for comparison. The values for $n = 9$ were taken from Ref. 16.

3. Barium

The natural isotopic mixture of Ba is composed of five even and two odd isotopes, both with the nuclear spin $I = 3/2$. The energy shifts of ^{135}Ba (6.59%) and ^{137}Ba (11.32%) $6sns\ ^1S_2$ states were analyzed between the principal quantum numbers $n = 21$ and $n = 50$ with respect to ^{138}Ba (71.66%).

The a_{6s} factors of Ba^+ are known accurately: a_{6s} ($^{135}Ba^+$) = 3.59167 GHz and a_{6s} ($^{137}Ba^+$) = 4.01887 GHz. Although the nuclear spins of both isotopes are identical, a slightly larger increase of the energy shift for ^{137}Ba should be obtained because of the larger value of a_{6s} for ^{137}Ba compared with ^{135}Ba. The comparison between experiment and theory is illustrated in Fig. 13 for both odd Ba isotopes. Again, the experimental data closely follow the theoretical predictions. The larger increase for ^{137}Ba is verified by the experiment. Deviations from the calculation for low n are due mainly to the influence of perturbing states such as $6p^2\ ^3P_0$, $5d6d\ ^3D_0$, and $5d6d\ ^1S_0$.[24] Specific mass and volume shifts are considerably affected by these perturbations. In addition, there are many more interacting levels in the Ba spectrum for high principal quantum numbers n, as can be seen from the work of Aymar *et al.*[29] and Aymar and Robaux.[30] These perturbations can lead to slightly different energy shifts because they are not included in this simple theory.

Detailed investigations of $6sns$ Rydberg series of Ba are given in Ref. 65. Exact knowledge of the hyperfine effects is necessary for the interpretation of configuration interaction in the presence of hyperfine interaction. Also, for the analysis of interaction between states from different principal quantum numbers n, information on hyperfine interaction within one n is essential, as will be shown in Subsection 4.D.

Hyperfine-induced state mixing leads not only to level shifts but also to changes in transition probabilities. Because J is no longer a good quantum number, states can be excited that normally could not be reached for reasons of selection rules. A typical example is the excitation of states belonging to the $5sns\ ^3S_1$ series in Sr with $50 < n < 85$ by Doppler-free two-photon transition from the $5s^2$ ground state because of the added transition strength from the admixed $5sns\ ^1S_0$ states.[66] This effect can, in principle, be

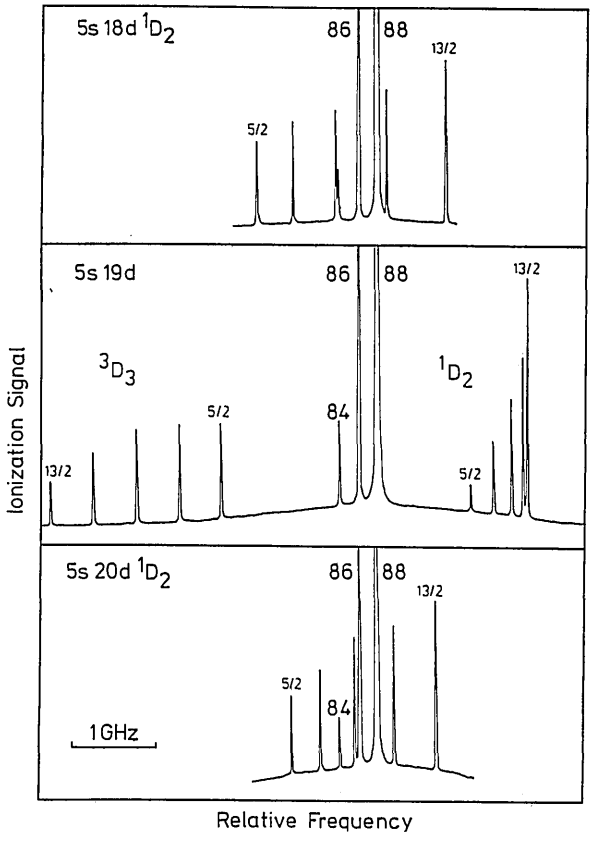

Fig. 14. Doppler-free spectra of the $5snd\ ^1D_2$ Rydberg series for n = 18, 19, 20. At n = 19 hyperfine transitions occur for the $^1D_2$ and $^3D_3$ states of ^{87}Sr.

used to investigate high Rydberg states that are not accessible from the ground state owing to selection rules.[67]

Both effects—level shifts and forbidden transitions—have been studied in the case of the hyperfine structure of the $5s19d\ ^1D_2$ state of ^{87}Sr.[68]

Figure 14 shows high-resolution two-photon spectra of the $5snd\ ^1D_2$ Rydberg state for principal quantum numbers n = 18, 19, 20. The three even isotopes of Sr are separated by an isotope shift dominated mainly by the mass effect. With increasing quantum number n, the relative position of the even isotopes remains constant. The odd isotope ^{87}Sr with the nuclear spin $I = 9/2$ exhibits a hyperfine structure characterized by the magnetic coupling constant A. The center of gravity of the hyperfine components is located between ^{86}Sr and ^{88}Sr for unperturbed states. At n = 19, however, the hyperfine structure is strongly perturbed, and two different structures on either side of the former center of gravity are detected. This perturbation is caused by the $5s19d\ ^3D_3$ level, which has approximately the same energy as the $5s19d\ ^1D_2$ state. The small energy difference between the $^1D_2$ and $^3D_3$ levels leads to a local singlet–triplet mixing introduced by the hyperfine interaction. Because of this mixing J is no longer a good quantum number at n = 19 for the odd isotope ^{87}Sr. Thus $5/2 < F < 13/2$ hyperfine levels of the $^3D_3$ state can be excited from the $F = 9/2$ ground state with two photons by $\Delta F = 0, \pm1, \pm2$ transitions. Transitions to the $F = 3/2$ and $F = 15/2$ components of the $^3D_3$ state correspond to a $\Delta F = \pm3$ transition and are not allowed in two-photon excitation. The strong interaction between hyperfine levels with the same F also causes an energy shift of the $^3D_3$ and $^1D_2$ hyperfine multiplets. The different signs of the hyperfine coupling constants A for singlet and triplet states and the fact that the strength of interaction increases with decreasing energy separation result in a violation of the hyperfine interval rule for both multiplets. The sum of the intensities for transitions to hyperfine levels with the same F gives the intensity ratios of the unperturbed n = 19 multiplet. This indicates that there are no additional strong perturbations around n = 19. When mixed wave functions are used, the hyperfine-induced energy shift can be included. The result is shown in Fig. 15.

If we neglect any perturbation by the $5s19d\ ^3D_3$ level and use the interpolated hyperfine coupling constant $A(^1D_2)$, a hyperfine multiplet, as shown in the upper part of Fig. 15, would be expected. By including the perturbation, the experimental data shown in the lower part of Fig. 15 can be described quantitatively, using the magnetic-dipole matrix

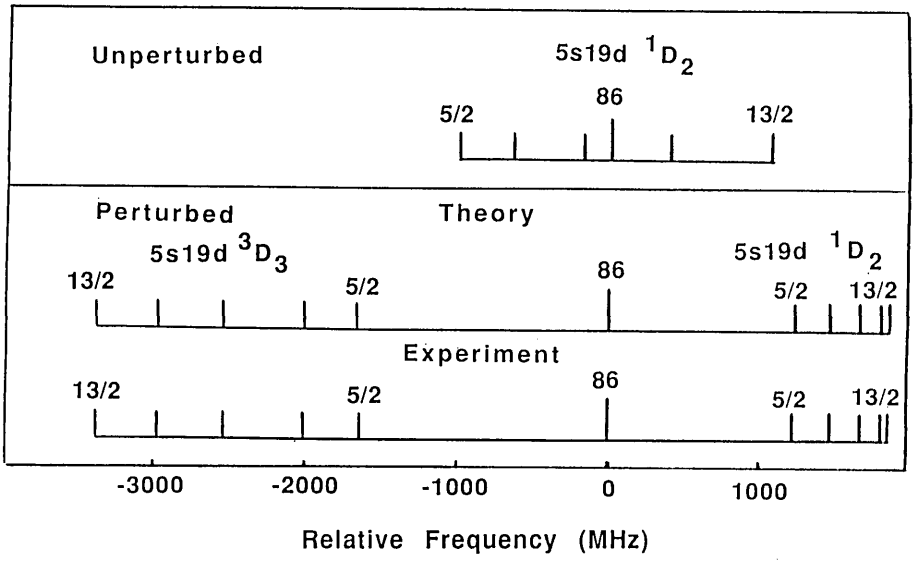

Fig. 15. Calculated hyperfine splitting of an unperturbed $5s19d\ ^1D_2$ state (upper part). A comparison between experiment and theory of the perturbed hyperfine multiplets of $5s19d\ ^1D_2$ and $^3D_3$ levels is shown in the lower part.

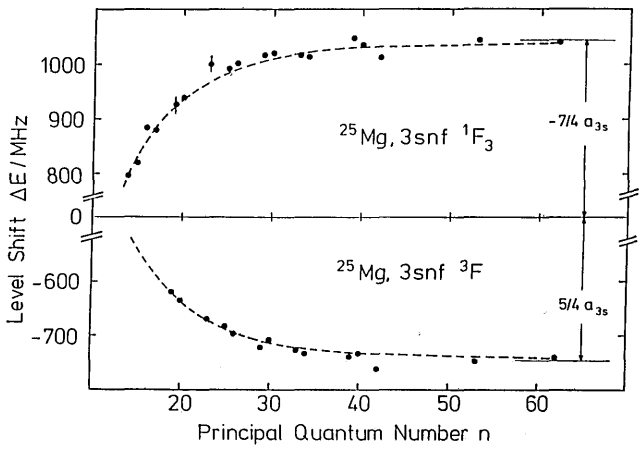

Fig. 16. Level shifts of the $3snf\,^{1,3}F$ Rydberg series of ^{25}Mg. Comparison between calculated energy shift (dashed curves, $F = 7/2$) and experimental data (points).

elements for an *sd* configuration in intermediate coupling. The maximum difference to the experimentally obtained transition energies was less than ±10 MHz.

For Mg, Doppler-free three-photon spectroscopy was applied to investigate the 3*snp* and 3*snf* Rydberg states up to the ionization limit.[69] Again level shifts and forbidden transitions were clearly observed. Figure 16 shows the measured level shifts of the $3snf\,F$ Rydberg series of ^{25}Mg. From these data the Fermi-contact term a_{3s} of the Mg ion was derived. This experiment demonstrates how measurements of the Rydberg states of the neutral atom can be used to determine constants of the ion. When the complete Rydberg series is used, the influence of screening effects that dominate for low-lying states need not be taken into account.

D. $a_{ms} = H_{0i}$

All effects described so far are limited to Rydberg states from the same principal quantum number n. In the third energy range under consideration the energy separation between levels belonging to different n is comparable with the Fermi-contact energy of the nonexcited s electron. In particular, the hyperfine components of singlet and triplet states from consecutive n are assumed to cross because of hyperfine-induced level shift, as described in Section 3. However, the hyperfine interaction causes these levels to repel each other, and an avoided crossing is observed. Such hyperfine-induced n mixing was determined experimentally, for the first time to our knowledge, in high Rydberg states of ^{87}Sr.[70] This effect is comparable with the anticrossing of Stark levels[71,72] or the avoided crossings induced by external magnetic fields.[73,74] It should be pointed out, however, that in the case of hyperfine-induced n mixing the internal magnetic fields of the nucleus alone produce the interaction leading to the anticrossing. It is thus an intrinsic feature of the atom and can be expected to occur in high Rydberg states of all two-electron systems.

A typical excitation spectrum between principal quantum numbers $n = 105$ and $n = 106$ is shown in Fig. 17, which shows transitions to the 5*sns* and 5*snd* Rydberg levels that were allowed by selection rules from the $5s^2\,^1S_0$ ground state. Transitions to the $^3S_1(F = I)$ component of ^{87}Sr and to the

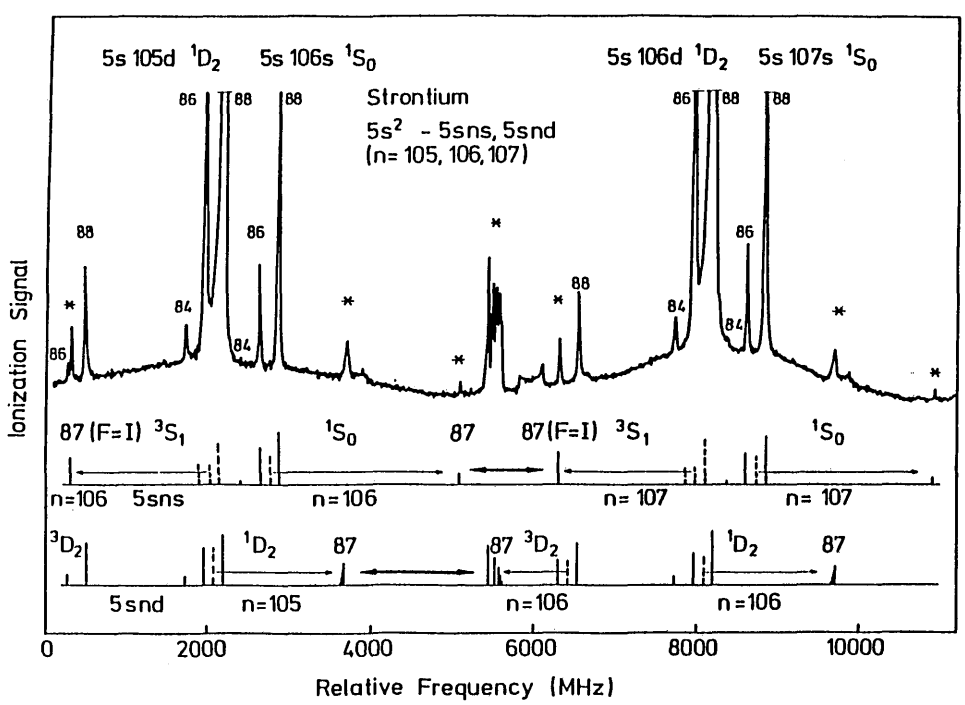

Fig. 17. Typical two-photon excitation spectrum of 5*sns* and 5*snd* Rydberg states of Sr. The even isotopes are labeled by their mass numbers; the intensities reflect their relative abundances (signals of ^{86,88}Sr are partly off scale). In the lower part the relative positions of signals from the 5*sns* and 5*snd* configuration are shown separately. Signals of the odd isotopes ^{87}Sr are marked by asterisks. Although in the 5*sns* series only one ^{87}Sr component ($F = I$) is excited, there are five hyperfine components ($F = 3/2 \ldots 13/2$) in the 5*snd* series. Horizontal arrows show the influence of hyperfine-induced level shifts of the odd isotope with respect to their unperturbed position (dashed lines). The heavier arrows indicate the hyperfine interaction between levels with different principal quantum numbers n.

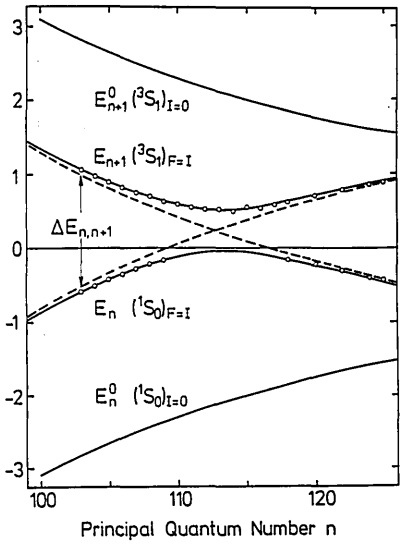

Fig. 18. Calculated avoided crossing between the $^1S_0(n)$ and $^3S_1(n+1)$ levels. The dashed curves represent behavior neglecting an interaction between states with different principal quantum numbers n. Open circles are experimentally determined level energies. The positions of $^1S_0(E_n{}^0)$ and $^3S_1(E^0_{n+1})$ levels without any hyperfine interaction are also indicated in order to demonstrate the large hyperfine-induced level shift.

hyperfine multiplet of the $^3D_2$ level of ^{87}Sr are caused by hyperfine-induced singlet–triplet mixing. The hyperfine-induced level shift is obvious for the $^1S_0$ and $^{1,3}D_2$ states. Let us first focus our discussion on the $5sns$ configuration. In the lower part of Fig. 17 the energy positions of the observed terms of the $5sns$ configuration are shown together with the positions of $^3S_1$ levels of ^{86}Sr and ^{88}Sr (dashed lines), which cannot be directly excited with two-photon transitions from the ground states. The wave functions of the admixed $^3S_1(F=I)$ and $^1S_0(F=I)$ levels have to be taken as a combination of pure LS-coupled wave functions:

$$|^1S_0, n, F\rangle = a_n|^1S_0, n, F\rangle^0 - b_n|^3S_1, n, F\rangle^0, \tag{7}$$

$$|^3S_1, n, F\rangle = a_n|^3S_1, n, F\rangle^0 + b_n|^1S_0, n, F\rangle^0. \tag{8}$$

Diagonalization of the Hamiltonian $H = H + a_{5s}sI$ results in the perturbed level energies of $^1S_0$ and $^3S_1(F = I)$ components.

In Fig. 18 (dashed lines) the expected energy-level shifts are shown for $^1S_0$ (principal quantum number n) and $^3S_1(F = I)$ (principal quantum number $n + 1$) levels in the interval $100 < n < 125$. For the calculation the singlet–triplet separation was adjusted to the experimental values at $n = 100$, where the interaction between different principal quantum numbers is negligible. It is obvious that the two perturbed levels belonging to principal quantum numbers n and $n + 1$ are supposed to cross.

However, if the energy separation, $\Delta E_{n,n+1}$, between the two levels becomes comparable with the Fermi-contact energy, a_{5s} (−0.99 GHz), they interact and repel each other. The new perturbed wave function $|\psi\rangle^*$ can be taken again as a linear combination of the two interacting levels

$$|^1S_0, n, F\rangle^* = a|^1S_0, n, F\rangle - b|^3S_1, n+1, F\rangle, \tag{9}$$

$$|^3S_1, n+1, F\rangle^* = a|^3S_1, n+1, F\rangle + b|^1S_0, n, F\rangle. \tag{10}$$

Diagonalization of the Hamiltonian $H = H_0 + a_{5s}sI$ in order to determine the perturbed energy levels requires the solution of matrix elements of type

$$\langle ^1S_0, n, F|a_{5s}sI|^3S_1, n+1, F\rangle. \tag{11}$$

The method used here has been described in detail elsewhere and has proved to be successful in the technique of isolated core excitation. The matrix element in Eq. (11) can be written as

$$\langle ^1S_0, F|a_{5s}sI|^3S_1, F\rangle\langle n^*|(n+1)^*\rangle, \tag{12}$$

where n^* and $(n+1)^*$ are effective quantum numbers of the $^1S_0$ and $^3S_1$ components, respectively. With the use of one-electron wave functions as calculated by Bhatti *et al.*,[75] the overlap integrals can be approximated by

$$\langle n^*/(n+1)^*\rangle = -\frac{2[n^*(n+1)^*]^{1/2}\sin\pi[(n+1)^* - n^*]}{n^* + (n+1)^*\pi[(n+1)^* - n^*]}. \tag{13}$$

With this approximation the perturbed level energies due to a hyperfine interaction between hyperfine levels from different n ($\Delta n = 1$) can be calculated, resulting in an avoided crossing comparable with the anticrossing of Stark levels. In Fig. 18 the calculated data are compared with experimentally determined energy levels. The agreement with calculation is excellent. Above the crossing the small deviation from the theoretical curve is caused by the interaction between energy levels with $\Delta n = 2$. The energy separation at $n = 125$ is already as small as 3.5 GHz. Between principal quantum numbers $110 < n < 118$ the $^1S_0$ component overlaps with the $^1D_2$ hyperfine multiplet, and only the $^3S_1(F = I)$ levels can be used for comparison.

The interaction described so far is not restricted to the

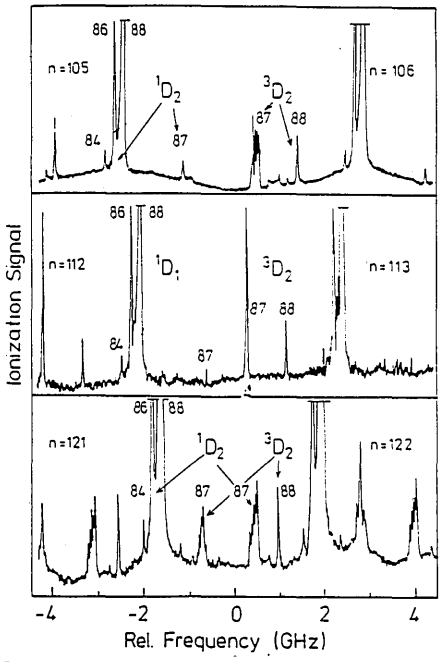

Fig. 19. Typical two-photon excitation spectra for three selected pairs of principal quantum numbers n, showing the hyperfine-induced n mixing for $5snd$ $^{1,3}D_2$ states. Above $n = 115$ the relative positions of the $^1D_2$ and $^3D_2$ hyperfine components are inverted, as indicated in the lower spectrum.

$5sns$ configuration. We have observed the same anticrossing for $^{1,3}D_2$ terms of the $5snd$ configuration. It also follows from the description given here that for higher n, anticrossings between hyperfine states differing in principal quantum number by $\Delta n = \pm 2$ or more will occur when the ionization limit is approached. We have observed a second crossing around $n = 140$ between $^1D_2$ and $^3D_2$ hyperfine multiplets of ^{87}Sr, which is also in agreement with our calculations.

Typical excitation spectra below, above, and at the anticrossing for $5snd\ ^{1,3}D_2$ levels are shown in Fig. 19. In addition to the strong repulsion of the hyperfine components of $^1D_2(n)$ and $^3D_2(n+1)$ levels of ^{87}Sr, there is a significant change in the transition probability. This can be explained in terms of the composition of the mixed wave functions. The mixed wave functions close to the crossing are symmetric and antisymmetric combinations of two wave functions, $|^1D_2, n, F\rangle$ and $|^3D_2, n+1, F\rangle$, which are composed of nearly equal amounts of singlet character owing to hyperfine-induced mixing within the same n. Therefore the singlet admixture in the antisymmetric wave function is near zero, whereas the symmetric wave function contains almost pure singlet character. Because only states with singlet and triplet character can be excited from the $^1S_0$ ground state, the intensity distribution in the crossing region should reflect the admixture. The experimentally observed intensities clearly confirm the expectation. The transition probability to the $^3D_2$ hyperfine components first increases when going from $n = 100$ to $n = 113$. After the crossing, the intensity of the $^3D_2$ signal decreases again, and both $^1D_2$ and $^3D_2$ hyperfine components can be excited.

5. CONCLUSIONS

The results presented here demonstrate how high-resolution spectroscopy can be exploited for the investigation and analysis of the electronic structure of Rydberg states of two-electron systems. In particular, the measurement of hyperfine structures is a highly sensitive probe for the determination of configuration interactions, state mixing, and hyperfine-induced singlet–triplet mixing. The coupling between the two electrons is crucially influenced by the admixture of other configurations and can easily be probed by the hyperfine structure. As a consequence, the hyperfine interaction can also be used as a probe in energy ranges of Rydberg series where it is not itself responsible for perturbations:

1. A resonancelike behavior in singlet–triplet mixing caused by configuration interaction was observed.
2. When hyperfine-structure data are used as additional input for MQDT calculations, these analyses can be improved considerably.
3. Even weak singlet–triplet mixing, far below 1%, was safely detected with the hyperfine interaction as the probe.
4. Localized configuration interaction can be treated quantitatively by means of hyperfine-structure measurements.

Hyperfine-induced perturbations become dominant whenever the separation between neighboring Rydberg states is smaller than or comparable with the Fermi-contact term of the low s electron. For high Rydberg states this will be the rule rather than the exception and has to be taken into account carefully. For an analysis of configuration interaction in the presence of hyperfine-induced effects, the exact knowledge of these effects is required. This is particularly the case for the heavier alkaline-earth element Ba.

Furthermore, the hyperfine-induced effects can be directly used for the investigation and analysis of high Rydberg states:

1. Hyperfine-induced state mixing also leads to changes in transition probabilities. As a consequence, states were excited that normally could not be reached because of selection rules.
2. From the determination of the hyperfine-induced energy-level shifts, the transition energies of unperturbed triplet states of even isotopes can be deduced.
3. In light alkaline-earth elements the hyperfine coupling constant of the ion ground states was evaluated from hyperfine-induced level shifts with high accuracy.

Finally, for high Rydberg states ($n > 100$), the energy separation between consecutive Rydberg states becomes comparable with the hyperfine splitting of the ion core. In this energy range the hyperfine interaction is again an ideal probe for the electronic structure of these rather exotic states:

1. A hyperfine-induced n mixing was observed for the first time in $5sns$ and $5snd$ Rydberg states for Sr.
2. Semiempirical calculations using one-electron product wave functions show excellent agreement with experiment.

ACKNOWLEDGMENTS

All research reported here were supported by the Deutsche Forschungsgemeinschaft. I wish to thank E. Matthias for numerous stimulating discussions, which essentially promoted the progress of the experiments. His continuous support and permanent interest also advanced the investigations crucially. I thankfully acknowledge the cooperation in both the experimental and theoretical part of the investigations by A. Timmermann, P. J. West, D. Schmidt, K. Lücke, and W. Makat. In particular, I would like to express my thanks to A. Timmermann for his high motivation during all parts of the research. The careful writing of the manuscript by A. Kuchenbecker is also thankfully acknowledged.

Although we were unable to complete the description of this study in time for its inclusion in the special issue of this journal celebrating the ninetieth birthday of Charlotte Moore Sitterly, we wish to associate our tribute to her with those that did appear in the special issue.

* Present address, Forschungsinstitut für Industrielle Bildverarbeitung, FIBH, Misburger Strasse 81, B 3000 Hannover 61, Federal Republic of Germany.

REFERENCES

1. K. Codling, Proc. R. Soc. London Ser. A **797**, 392 (1960).
2. G. Risberg, Ark. Fys. **28**, 381 (1964).
3. J. W. Swensson and G. Risberg, Ark. Fys. **31**, 237 (1965).
4. G. Risberg, Ark. Fys. **37**, 231 (1967).

5. C. M. Brown, S. G. Tilford, and M. L. Ginter, J. Opt. Soc. Am. **63,** 1454 (1973).
6. W. R. S. Garton, J. Quant. Spectrosc. Radiat. Transfer **2,** 235 (1978).
7. D. J. Bradely, P. Ewart, J. V. Nicholas, and J. R. D. Shaw, J. Phys. B **8,** 2934 (1975).
8. C. M. Brown, R. H. Naber, S. G. Tilford, and M. L. Ginter, Appl. Opt. **12,** 1858 (1973).
9. P. Ewart, Phys. Lett. **61A,** 383 (1977).
10. P. Esherick, J. A. Armstrong, R. W. Dreyfus, and J. J. Wynne, Phys. Rev. Lett. **36,** 1296 (1975).
11. P. Camus, J. Phys. B **7,** 1154 (1974).
12. J. R. Rubbmark and S. A. Borgström, Phys. Scr. **18,** 196 (1978).
13. P. Ewart and A. F. Purdie, J. Phys. B **9,** 437 (1976).
14. P. Camus, M. Dieulin, and A. El Himdy, Phys. Rev. A **26,** 379 (1981).
15. D. J. Bradley, P. Ewart, J. V. Nicholas, and J. R. D. Shaw, J. Phys. B **6,** 1594 (1973).
16. J. R. Rubbmark, S. A. Borgström, and K. Borgkasten, J. Phys. B **10,** 421 (1977).
17. D. Camus and C. Morillon, J. Phys. B **10,** L133 (1977).
18. S. A. Borgström and J. R. Rubbmark, J. Phys. B **10,** 3607 (1977).
19. R. Beigang and D. Schmidt, Phys. Lett. **87A,** 21 (1981).
20. R. Beigang, K. Lücke, D. Schmidt, and A. Timmermann, Phys. Scr. **26,** 183 (1982).
21. K. H. Kingdon, Phys. Rev. **21,** 408 (1923).
22. D. Popescu, F. Popescu, and J. Richter, Z. Phys. **226,** 160 (1969).
23. B. Stoicheff, *Laser Spectroscopy* (Springer-Verlag, Berlin, 1981), p. 229.
24. M. J. Seaton, Proc. Phys. Soc. (London) **88,** 801 (1966).
25. K. T. Lu, J. Opt. Soc. Am. **64,** 706 (1973).
26. J. A. Armstrong, P. Esherick, and J. J. Wynne, Phys. Rev. A **15,** 180 (1977).
27. J. A. Armstrong, J. J. Wynne, and P. Esherick, J. Opt. Soc. Am. **69,** 211 (1978).
28. P. Esherick, Phys. Rev. A **15,** 1920 (1977).
29. M. Aymar, P. Camus, M. Dieulin, and C. Morillon, Phys. Rev. A **18,** 2173 (1978).
30. M. Aymar and O. Robaux, J. Phys. B **12,** 53 (1978).
31. M. Aymar and P. Camus, Phys. Rev. A **28,** 850 (1983).
32. P. Grafström, Jiang Zhan-Kui, G. Jönsson, S. Kröll, C. Levinson, H. Lundberg, and S. Svanberg, Z. Phys. A **306,** 281 (1982).
33. W. E. Cooke, "Two electron rydberg states," in *Atomic Physics 7,* D. Kleppner and M. F. Pipkin, eds. (Plenum, New York, 1981), p. 167.
34. K. Bhatia, P. Grafström, C. Levinson, H. Lundberg, L. Nilsson, and S. Svanberg, Z. Phys. A **303,** 1 (1981).
35. T. F. Gallagher, W. Sandner, and K. A. Safinya, Phys. Rev. A **23,** 2969 (1981).
36. M. Aymar, R.-J. Champeau, C. Delsart, and J. C. Keller, J. Phys. B **14,** 4489 (1981).
37. M. Aymar, P. Grafström, C. Levinson, H. Lundberg, and S. Svanberg, J. Phys. B **15,** 877 (1982).
38. W. Gornik, Z. Phys. A **283,** 231 (1977).
39. P. Grafström, Jiang Zhan-Kui, G. Jönssen, C. Levinson, H. Lundberg, and S. Svanberg, Phys. Rev. A **27,** 347 (1983).
40. G. Gessert, P. Kulina, and R.-H. Rinkleff, J. Phys. B **16,** L313 (1983).
41. W. Hogervorst, Commun. At. Mol. Phys. **13,** 68 (1983).
42. J. J. Wynne, J. A. Armstrong, and P. Esherick, Phys. Rev. Lett. **39,** 1520 (1977).
43. P. Grafström, C. Levinson, H. Lundberg, S. Svanberg, P. Grundevik, L. Nilson, and M. Aymar, Z. Phys. A **308,** 95 (1982).
44. H. Gerhardt, F. Jeschonnek, W. Makat, F. Schneider, A. Timmermann, R. Wenz, and P. J. West, Appl. Phys. **22,** 361 (1980).
45. R. Beigang, K. Lücke, A. Timmermann, and P. J. West, Opt. Commun. **42,** 19 (1982).
46. G. Grynberg and B. Cagnac, Rep. Prog. Phys. **40,** 791 (1969). See also W. Demtröder, *Laser Spectroscopy,* Vol. 5 of Springer Series in Chemical Physics (Springer-Verlag, Berlin, 1981).
47. K. C. Harvey, Rev. Sci. Instrum. **52,** 104 (1981).
48. K. Niemax, Acta Phys. Pol. A **61,** 517 (1982).
49. J. Neukammer and H. Rinneberg, J. Phys. B **15,** 2899 (1982).
50. U. Majewski, J. Neukammer, and H. Rinneberg, Phys. Rev. Lett. **51,** 1340 (1983).
51. W. Hogervorst, Comments At. Mol. Phys. **13,** 69 (1983).
52. E. R. Eliel, Ph.D. dissertation (Vrije Universiteit, Amsterdam, 1982).
53. E. R. Eliel, W. Hogervorst, T. Olsson, and L. R. Pendrill, Z. Phys. A **311,** 1 (1983).
54. E. R. Eliel and W. Hogervorst, J. Phys. B **16,** 188 (1983).
55. E. R. Eliel and W. Hogervorst, Phys. Rev. A **27,** 2995 (1983).
56. J. Neukammer, H. Rinneberg, K. Vietzke, A. König, H. Hieronymus, M. Kohl, and H.-J. Grabka, Phys. Rev. Lett. **59,** 2947 (1987).
57. H. Rinneberg, J. Neukammer, G. Jönsson, H. Hieronymus, A. König, and K. Vietzke, Phys. Rev. Lett. **55,** 382 (1985).
58. R. Beigang, K. Lücke, and A. Timmermann, Phys. Rev. A **27,** 587 (1983).
59. R. Beigang, E. Matthias, and A. Timmermann, Phys. Rev. Lett. **47,** 326 (1981).
60. H. Rinneberg and J. Neukammer, Phys. Rev. Lett. **49,** 124 (1982).
61. H. Rinneberg and J. Neukammer, Phys. Rev. A **27,** 1779 (1983); J. Neukammer and H. Rinneberg, J. Phys. B **15,** L723, L825 (1982).
62. H. Kopfermann, *Nuclear Moments* (Academic, New York, 1958).
63. P. F. Liao, R. R. Freeman, R. Panock, and L. M. Humphrey, Opt. Commun. **34,** 195 (1980).
64. L. Barbier and L. Champeau, J. Phys. (Paris) **41,** 947 (1980).
65. H. Rinneberg, J. Neukammer, and E. Matthias, Z. Phys. A **306,** 11, (1982); J. Neukammer and H. Rinneberg, J. Phys. B **15,** L425 (1982).
66. R. Beigang and A. Timmermann, Phys. Rev. A **25,** 1496 (1982).
67. R. Beigang and A. Timmermann, Phys. Rev. A **26,** 2990 (1982).
68. R. Beigang, D. Schmidt, and A. Timmermann, J. Phys. B **15,** L201 (1982).
69. R. Beigang, D. Schmidt, and A. Timmermann, Phys. Rev. A **28,** 2581 (1984).
70. R. Beigang, W. Makat, A. Timmermann, and P. J. West, Phys. Rev. Lett. **9,** 771 (1983).
71. M. L. Zimmermann, M. G. Littmann, M. M. Kash, and D. Kleppner, Phys. Rev. A **20,** 2251 (1979).
72. P. Cacciani, E. Luc-Koenig, J. Pinard, C. Thomas, and S. Liberman, Phys. Rev. Lett. **56,** 1124 (1986).
73. J. C. Castro, M. L. Zimmermann, R. G. Hulet, D. Kleppner, and R. R. Freeman, Phys. Rev. A **45,** 1780 (1980).
74. J. R. Rubbmark, M. M. Kash, M. G. Littmann, and D. Kleppner, Phys. Rev. A **23,** 3107 (1981).
75. S. A. Batthi, C. L. Cromer, and W. E. Cooke, Phys. Rev. A **24,** 161 (1981).